



Effect of channel confluence on the dynamics of debris flow in the Niutang Gully

Hao Wang¹ · Jintao Zhang¹ · Qing Hu² · Wei Liu³ · Liqun Ma⁴

Received: 24 April 2024 / Accepted: 1 August 2024
© The Author(s), under exclusive licence to Springer Nature B.V. 2024

Abstract

Debris flows are dangerous, rapid, and often observed in precipitous landslides comprising water-laden soil, rock, and debris. Moreover, under the influence of large-scale precipitation, the occurrence of debris-flow clusters may lead to confluence, altering their movement dynamics and the extent of their impact. Such events present a substantial risk to human life and safety, as well as causing severe damage to the ecological environment near the flow channels; however, the dynamic processes during debris flow confluence remain poorly understood. Here, we numerically simulated the flow process of debris flows based on observational data of the August 19–20, 2011 (“8.20”) debris flow in the Niutang Gully. Additionally, the investigation examined how the number of channels and the angles between channels at the confluence location affect the movement characteristics of post-confluence debris flow. The results indicated that upon the confluence of channelized debris flows, the velocity and deposition height of the debris flow vary with changes in the confluence angles. As the angle between the channels in the confluence area increases, so does the height of the sediment deposition, while the speed of the debris flow is reduced. Furthermore, the confluence angles affected the morphology of the debris flow deposition. As the confluence angle increased, so did the length of the debris-flow deposit fan, while the breadth was reduced. These findings show that the confluence has a substantial impact on the movement characteristics of debris flows, and this information may serve as a theoretical reference for debris-flow protection engineering.

Keywords Debris flow · Numerical simulation · Confluence · Movement characteristics

✉ Wei Liu
spon@imde.ac.cn

¹ School of Civil Engineering and Architectural, Henan University, Kaifeng, China

² School of Civil Engineering, Shangqiu Institute of Technology, Shangqiu, China

³ Institute of Mountain Hazards and Environment, Chinese Academy of Sciences, Chengdu, China

⁴ The College of Geography and Environmental Science, Henan University, Kaifeng, China

1 Introduction

Debris flows are a highly destructive and specialized type of flood, the formation of which is influenced by both natural processes and human activities (Cheng et al. 2018; Trujillo-Vela et al. 2022). Debris flows and sediments impact human life and property, destroy vegetation, and affect the growth of plants in water systems (Silva et al. 2022; Wang et al. 2022a). In mountainous regions, heavy rainfall may cause debris flows in multiple tributaries simultaneously, which then converge into the main channel, exerting significant destructive power (Ma et al. 2013). For example, in 2010, two channels in Zhouqu County, Sichuan, experienced large-scale debris flows that subsequently converged, resulting in the deaths of over a thousand people (Tang et al. 2011; Wang 2013; Zhang and Matsushima 2016). The Niujian Gully debris flow system in Wenchuan County consists of a main channel and six tributaries. Following the 2008 Sichuan earthquake, a devastating debris-flow disaster occurred that caused immense destruction. It buried roads and blocked the Minjiang River, putting the lives of over 1,100 people at risk (Yang et al. 2023). Additionally, debris flow confluence has occurred in regions such as Jiangjia (Chen et al. 2005; Guo et al. 2020; Li et al. 2015) and Niwan Gullies (Ouyang et al. 2019; Ma and Liu 2022). A thorough understanding of the influence of confluence on the movement characteristics of debris flows would therefore be beneficial for guiding land development, utilisation, and planning to reduce social impacts.

The phenomenon of debris flow convergence has garnered significant scholarly attention. Results from flume tests and simulation experiments indicate that when a debris flow emerges from a gully and intersects with the main river, the likelihood of river blockage is complexly influenced by the particle size composition, density, and flow rate of the debris flow. The interweaving effect of multiple factors, including the total volume and the topography of the intersection area, further complicates this process (Du 2021; Du et al. 2014; Liu et al. 2021b; Dang et al. 2009; Wang et al. 2022c). Notably, the convergence angle is a key indicator for assessing the risk of debris flow channel blockage. Its magnitude is directly related to changes in the velocity component perpendicular to the main flow direction, profoundly affecting the dynamic interaction and material exchange processes between the debris flow and the main flow (Dang et al. 2009). Additionally, when tributaries merge into the mainstream at a specific angle, the flow rate of the mainstream accelerates, enhancing the transport efficiency of the debris flow and promoting the downstream migration of more solid materials, thereby reducing the likelihood of significant blockage in the main river (Zhang et al. 2015). Further complicating this process, when debris flows in two adjacent channels merge into the main river almost simultaneously or sequentially, the angle between the two streams and the sequence of their inflows become determining factors for the migration pattern and accumulation of debris flow materials in the main river. These factors ultimately affect the morphological characteristics of the accumulation fan formed in the confluence area (Stancanelli et al. 2014, 2015; Chen et al. 2017). Overall, previous research has predominantly focused on the morphological changes in debris flow accumulation fans following confluence as well as the potential occurrence of damming events. Moreover, studying the motion characteristics and flow extent of debris flows is a focal point in disaster prevention and mitigation research, as these factors determine the hazards associated with debris flows. Notably, confluence phenomena can significantly influence the motion characteristics of debris flows (Chang et al. 2017; Lin et al. 2011). However, explo-

ration of the dynamic processes occurring when multiple debris flows undergo confluence within the flow channel has been limited.

Debris flow outbreaks exhibit a stochastic nature; thus, obtaining convergence data from field surveys is challenging (Chen 2000; Cui et al. 2018). Additionally, studying the dynamic characteristics of debris flow convergence involves multiple channels, making it difficult to accurately collect the required data. In recent years, numerical simulation has become an important method for studying debris flow and its dynamics (Wang et al. 2018). Among commonly used numerical simulation software for debris flows (Chen et al. 2018; Ding et al. 2023; Horton et al. 2019), the simulation accuracy of Rapid Mass Movement Simulation (RAMMS) software, developed by the Swiss Institute for Snow and Avalanche Research, has been validated across various research areas (Mikoš et al. 2021). RAMMS software enables the convenient definition of multiple source and erosion areas on the ground model, with parameters set individually for each. Moreover, RAMMS offers two modes for the initiation of debris flows: block and hydrological release, with the hydrological release curve customizable based on actual observation data. These features improve the correspondence of the debris flow simulation results from RAMMS to observed real-life conditions. Additionally, RAMMS can directly output simulation results as 3D animations, allowing for intuitive visualization of flow height, velocity, and other data at every moment of the debris flow process on a terrain map, facilitating subsequent data extraction and analysis (Liu et al. 2021a).

The confluence of debris flows in the transportation zone substantially affects the movement characteristics, triggering strong erosion and collapse at the bottom and sides of the channel, rendering the resulting debris flow more impactful and destructive. The aim of this study was to conduct an in-depth study on this topic. Initially, the basic characteristics of debris flows in the Niutang Gully were collated according to geographical, geological, and meteorological perspectives, and the parameters for simulations were obtained from field surveys. Using RAMMS software, different channel outbreaks and confluences of debris flows in the Niutang Gully were simulated, and velocity–depth curves were plotted accordingly. Finally, the influence of confluence angles on the movement characteristics of channel-type debris flows was explored through flume simulation experiments, followed by further analysis of the movement characteristics observed during the confluence of debris flows in the Niutang Gully.

2 Study area

2.1 Topography and landforms

The Niutang Gully is situated in Shuimo Town, Wenchuan County, Sichuan Province (Fig. 1). The overall drainage pattern resembles a branching structure with a total basin area of 23.53 km². The terrain within the watershed is steep with slopes generally exceeding 50°. The average longitudinal slope of the channel is 210‰ (Table 1), providing excellent conditions for rainfall runoff. The study area and its surrounding topography are primarily mid-mountainous, followed by low hills and river valleys. As depicted in Fig. 1b, the maximum altitude within the study region is 2440 m, whereas the confluence of the Niutang Gully with the Shou River is at the lowest point with an elevation of 900 m. The breadth of the

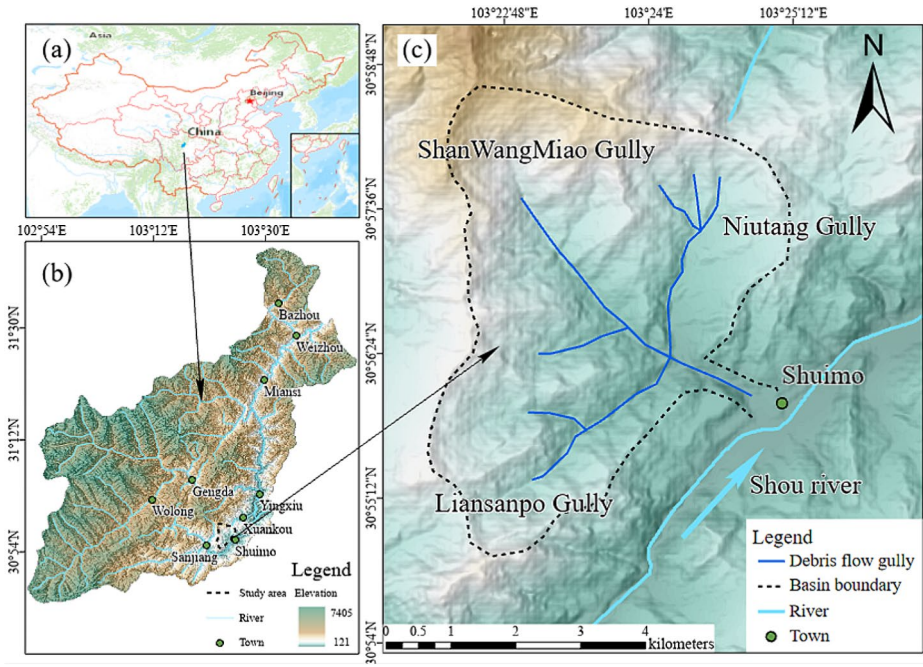


Fig. 1 Location of the Niutang Gully. **(a)** Location within China. **(b)** Location within Wenchuan County. **(c)** Locations of the Niutang Gully and its tributaries, and the surrounding environment distribution

Table 1 Topographic parameters of the three gullies

Channel characteristics	Length (km)			Width (m)			Average longitudinal slope (‰)		
	A*	B*	C*	A*	B*	C*	A*	B*	C*
Confluence zone of clearwater	1.49	0.835	1	3–18	5–20	3–15	330	249.4	597.7
Source-transport zone	3.12	3.854	5	7–60	20–90	10–70	110	87.36	72.4
Depositional zone	/	/	0.15	/	/	/	/	/	41.3
Grand total	4.61	4.689	6.15	/	/	/	266	74	116

*A, B, and C denote the three debris flow channels: A, ShanWangMiao Gully; B, Liansanpo Gully; and C, Niutang Gully. “/” indicates no data

gully bed ranges from 10 to 100 m (Table 1), often exhibiting a “U”-shape on cross-section. The slopes in the study area exhibit considerable variability, with longitudinal slopes of the gully bed ranging from 100 to 400‰, averaging around 250‰. The slopes on both sides of the channel are predominantly in the range of 52° to 86°, with the steepest slopes approaching 90°. The significant variation in slope in the study area leads to frequent landslides and subsidence, which in turn provide ample sediment sources for debris flow in the channel.

2.2 Geological and climate setting

Niutang Gully is located in the central-southern segment of the Huaxia tectonic belt of the Jiuding Mountains. Additionally, it belongs to the intermontane fold-and-thrust belt between the Ganzi–Songpan sag and the Yangtze Craton, exhibiting a structurally complex setting. The geological formations in the research area include Quaternary deposits (Q_4^{el+dl} , Q_4^{col+dl} , Q_4^{sef} , Q_4^{2del}) and the Devonian Woguanshan Formation. The primary soil types are composed of debris flow deposits containing gravelly soil, blocky gravelly soil formed by landslides, and silty clay with gravel deposits derived from residual slope accumulation.

Wenchuan County experiences a mountainous subtropical humid monsoon climate with substantial variations in topography and elevation, which contributes to distinct climate zones. The region has well-defined vertical climate zones, resulting in distinct seasons and relatively mild extreme temperatures in both winter and summer, providing favorable conditions for crop growth. Figure 2 shows the annual precipitation pattern in the Shuimo area, showing that the majority of rainfall occurs from June to September. This time interval constitutes around 65% of the total annual rainfall. The average annual precipitation from 2011 to 2015 was 1253.1 mm, with the highest recorded annual precipitation reaching 1688 mm and the lowest recorded at 836.7 mm.

2.3 Occurrence of the debris flow

The Niutang Gully is an ancient debris flow channel that has experienced five distinct geological disasters of debris flow since the 1960s. The most recent event occurred on August 20, 2011 (the “8.20” event). From 8:00 PM on August 19 to 8:00 AM on August 20, heavy rainfall was widespread in the Xuanying area of Wenchuan County. Shuimo Town received 157.2 mm of rainfall during this period, triggering numerous landslides on both sides of the gully. This led to a substantial increase in sediments in the Niutang Gully, resulting in a large-scale debris flow. According to measurements of the debris flow traces, the velocity of the flow within the channel from the starting point to the exit point reached 250.07 m³/s during the 8.20 event. The debris flow engulfed Niutang Village, damaging agricultural land, and infrastructure, including residences, roadways, water and electricity systems, and communication networks.

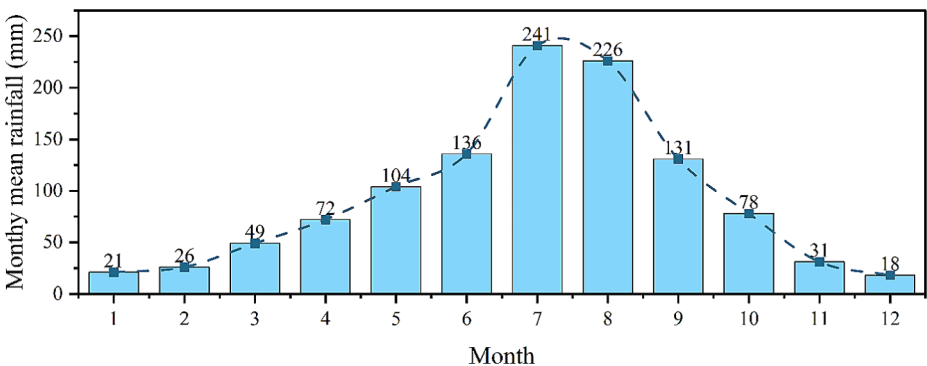


Fig. 2 Monthly average precipitation in the Shuimo area from 2011 to 2015

It is noteworthy that the economic activities of the local population have affected the topographical environment. This is primarily manifested in the construction of buildings, roads, and terrace farming in relatively flat channels. The phenomenon of structures encroaching on river channels is particularly pronounced, with the water plant in Shuimo Town being built on the left bank of the confluence of the Niutang and ShanWangMiao Gullies, occupying approximately one-third of the channel. During the 8.20 debris flow event, the sediment accumulation within the water plant reached a thickness of 1.5 to 2 m, as shown in Fig. 3c. Both the water plant and houses encroaching on the channel along the gully were severely affected by this debris flow. There are 14 bridges and culverts in the village, nine of which are of the type shown in Fig. 3d. These structures hinder the movement of debris flow in the channel, resulting in siltation and the submersion of more than 300 houses.

3 Numerical Model

3.1 Voellmy–salm fluid model

The motion-control model employed by the RAMMS software for debris flows was the Voellmy–Salm fluid model. This model postulates that debris flows are unsteady and non-homogeneous fluids for computational purposes (Christen et al. 2010; Deubelbeiss and Graf 2013).



Fig. 3 The occurrence of debris flow in the Niutang Gully. **(a)** Debris flow source generated by collapse. **(b)** Debris flow source generated by landslides. **(c)** The water treatment plant was inundated by the 8.20 debris flow. **(d)** Encroachment of buildings upon the debris flow channel

This system’s velocity is represented as:

$$U(x, y, t) = [U_x(x, y, t), U_y(x, y, t)]^T \tag{1}$$

where U_x is the velocity in the x-direction, U_y is the velocity in the y-direction, and T is the transpose matrix of the average velocity.

The magnitude of the velocity is:

$$\|U\| = \sqrt{U_x^2 + U_y^2} \tag{2}$$

$$n_u = \frac{1}{\|U\| (U_x, U_y)} \tag{3}$$

where $\|U\|$ is the absolute mean value of the velocity, ensuring that the velocity U is positive in the vector space. In Eq. (3), n_u represents the direction of the fluid velocity.

The flow height is:

$$\partial_t H + \partial_x (HU_x) + \partial_y (HU_y) = Q(x, y, t) \tag{4}$$

where $Q(x, y, t)$ represent the accumulation quantity and H represents the accumulation height.

The frictional resistance S_f is determined by the friction forces acting in the x- and y -directions, which can be expressed as follows:

$$S_f = (S_{fx} + S_{fy}) = nU_x \left[\mu g_z H + \frac{g\|U\|^2}{\zeta} \right] + nU_y \left[\mu g_z H + \frac{g\|U\|^2}{\zeta} \right] \tag{5}$$

$$S_{fx} = nU_x \left[\mu g_z H + \frac{g\|U\|^2}{\zeta} \right] \tag{6}$$

$$S_{fy} = nU_y \left[\mu g_z H + \frac{g\|U\|^2}{\zeta} \right] \tag{7}$$

The fluid height balance equations can be expressed as:

$$\partial_t (HU_x) + \partial_x \left(C_x HU_x^2 + g_z K_{\alpha/P} \frac{H^2}{2} \right) + \partial_y (HU_x U_y) = S_{gx} - S_{fx} \tag{8}$$

$$\partial_t (HU_y) + \partial_y \left(C_y HU_y^2 + g_z K_{\alpha/P} \frac{H^2}{2} \right) + \partial_x (HU_x U_y) = S_{gy} - S_{fy} \tag{9}$$

where C_x and C_y are the section coefficients, and g_z is the gravitational acceleration in the vertical direction.

Using the aforementioned equations, the Voellmy rheological formula can be derived as:

$$\frac{d(Uh)}{dt} = (z \cdot n)nh - k(\nabla h)h - \left[\mu(z \cdot n)h + \frac{1}{z\epsilon\eta}U^2 \right]s \tag{10}$$

3.2 Determining simulation parameters for RAMMS

The RAMMS software was used to simulate the confluence movement of debris flows. Prior to the simulation, the geographical data of the Niutang Gully were preprocessed using ArcGIS mapping software (Wang et al. 2022b), which involved converting the elevation data into ASCII files. Subsequently, the geographical model information for the Niutang Gully was imported into RAMMS. We conducted two field surveys in the area before and after the debris flow occurred and obtained the ground model data and source distribution data required for numerical simulation with a ground model accuracy of 5 m to meet the research requirements. The simulation parameters were set according to the guidelines provided in the RAMMS manual. Finally, the simulated results of the debris flow were compared with historical debris flow events. The simulation parameters were iteratively calibrated until the simulated results closely matched the actual outcomes, as depicted in Fig. 4.

The parameters to be determined for numerical simulation using RAMMS include the turbulent coefficient ξ , dry friction coefficient μ , and erosion information. Particularly, the selection of ξ and μ can markedly affect the flow process of debris flows (Wang et al. 2022b). The values of ξ and μ were chosen within the recommended range specified in the software user manual. After multiple reverse simulations of debris flows, the final values for ξ and μ were determined to be 700 and 0.09, respectively. Based on the actual erosion conditions in Niutanggou, two erosion areas were defined in the simulation, as illustrated in Fig. 4. The red area indicates that the channel material in this region is easily eroded, with a potential erosion depth parameter of 0.2, whereas the blue area denotes that the channel material is more resistant to erosion, with a potential erosion depth parameter of 0.1. The remaining parameters for both areas are consistent, with an erosion density of 2000 kg/m³, an erosion rate of 0.0250 m/s, a critical shear stress of 1 kPa, and no limit on the maximum erosion depth. The corresponding simulation results for the 8.20 debris flow are depicted in

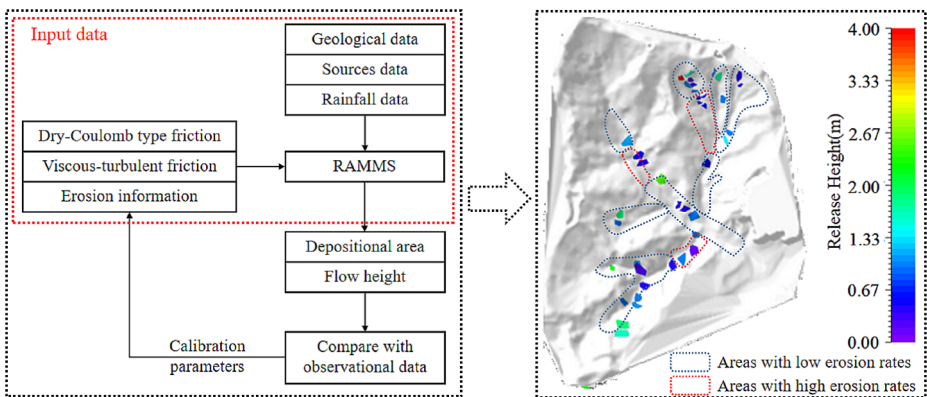


Fig. 4 Establishing the ground model and determining parameters

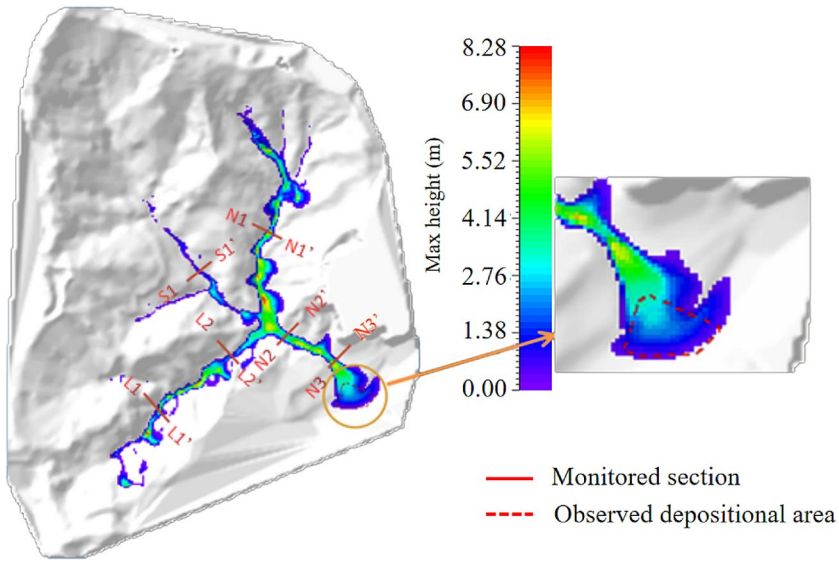


Fig. 5 Comparison of simulation results and field observations

Fig. 6 Comparison of cross-section debris flow accumulation height

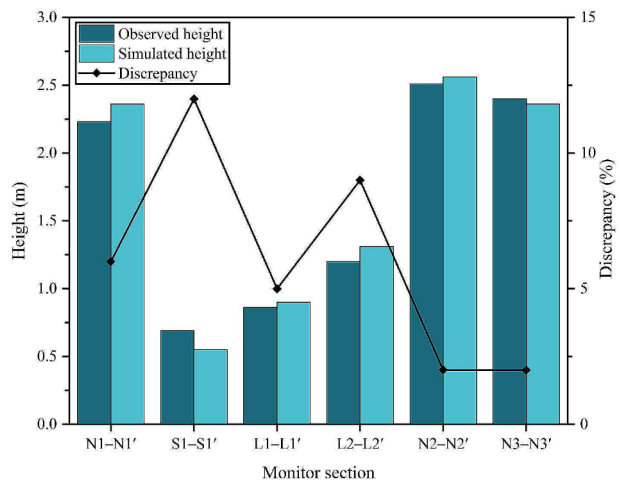


Fig. 5. Six cross-sections were selected from the Niutang Gully Basin for further validation of the accuracy of the chosen simulation parameters. The comparative results for the local cross-sectional debris-flow accumulation heights are presented in Fig. 6. Figure 5 provides visual evidence that the final accumulation range simulated by RAMMS is essentially consistent with the 8.20 debris flow. Moreover, Fig. 6 illustrates that the numerical simulation results of the six selected cross sections differ by only 12% from the actual maximum debris flow occurrence, demonstrating the appropriateness of the chosen numerical simulation parameters.

The discharge of debris flows and the number of channels involved in the confluence can affect flow dynamics. Accordingly, we investigated the motion properties of debris flows

in the Niutang Gully under the circumstances of simultaneous eruption and convergence in multiple channels.

Precipitation is an important factor for the formation of debris flows, with different rainfall amounts corresponding to varying debris flow magnitudes. Therefore, when simulating the confluence of different channels, the differential factors of rainfall should be considered. In this study, during the simulation of single-channel flow and the convergence of two or three channels, respective rainfall amounts corresponding to 10%, 5%, and 3.33% of the storm frequency were selected. The debris flow hydrographs required for software simulation were calculated using the equations provided in the “Hydrology Handbook of Sichuan Province” as follows:

$$Q_p = 0.278 \left(\frac{S}{\tau^n} - \mu_r \right) F \tag{11}$$

$$Q_{pc} = (1 + \phi_c) Q_p \tag{12}$$

where Q_p is the peak flow of the rainstorm, S is the designed rainstorm parameter, and n is the index representing rainfall intensity in the rainstorm formula. These data were obtained by consulting local hydrological manuals. τ is the time of rainwater confluence, calculated through comprehensive confluence considerations. μ_r is the runoff coefficient, and F is the confluence area in the region, whereas ϕ_c serves as the sediment correction coefficient. Table 2 summarizes the characteristics and hydrological parameters of the seven scenarios used in debris flow simulations.

*The symbol “+” indicates simultaneous occurrence and confluence of multiple debris flows. For example, A+B represents the simultaneous eruption and confluence of Channels A and B. A, ShanWangMiao Gully; B, Liansanpo Gully; and C, Niutang Gully.

4 Results and discussion

4.1 Simulation of the confluence of the Niutanggou debris flow

Figure 7 illustrates the flow height of debris flows occurring in various tributaries of Niutanggou. The data reveal that the movement range of debris flows when three tributaries experience simultaneous flow is greater than when any two tributaries are involved. Simi-

Table 2 Hydrological parameters for different scenarios

Scenario	Probability of rainfall occurrence (P)	Peak flow of the rainstorm Q_p (m ³ /s)	Peak debris flow Q_{pc} (m ³ /s)	Total volume of debris flow (m ³)
A	10%	53.51	122.25	48,300
B	10%	95.59	113.66	44,900
C	10%	58.79	204.08	80,400
A+B*	5%	183.06	279.74	132,700
A+C*	5%	176.87	387.27	211,700
B+C*	5%	133.27	377.13	206,000
A+B+C*	3.33%	262.78	556.38	285,400

larly, the movement range when any two tributaries experience simultaneous flow exceeds that observed in a single tributary. This indicates that debris flows occurring in multiple tributaries increase both the movement range and the potential for damage, thereby elevating the overall risk.

To gain a detailed understanding of the post-confluence movement characteristics of debris flows, the downstream channel of the Niutang Gully (highlighted by the blue solid line in Fig. 8) was chosen to study the variations in flow velocity and height after the confluence of the debris flows from the three gullies. The downstream channel was approximately 1920 m in length.

Figure 9 illustrates the accumulation height of the downstream gully debris flow under different confluence conditions. It is evident from the figure that the flow distance markedly increases after the confluence of the debris flows. The figure illustrates that both the flow

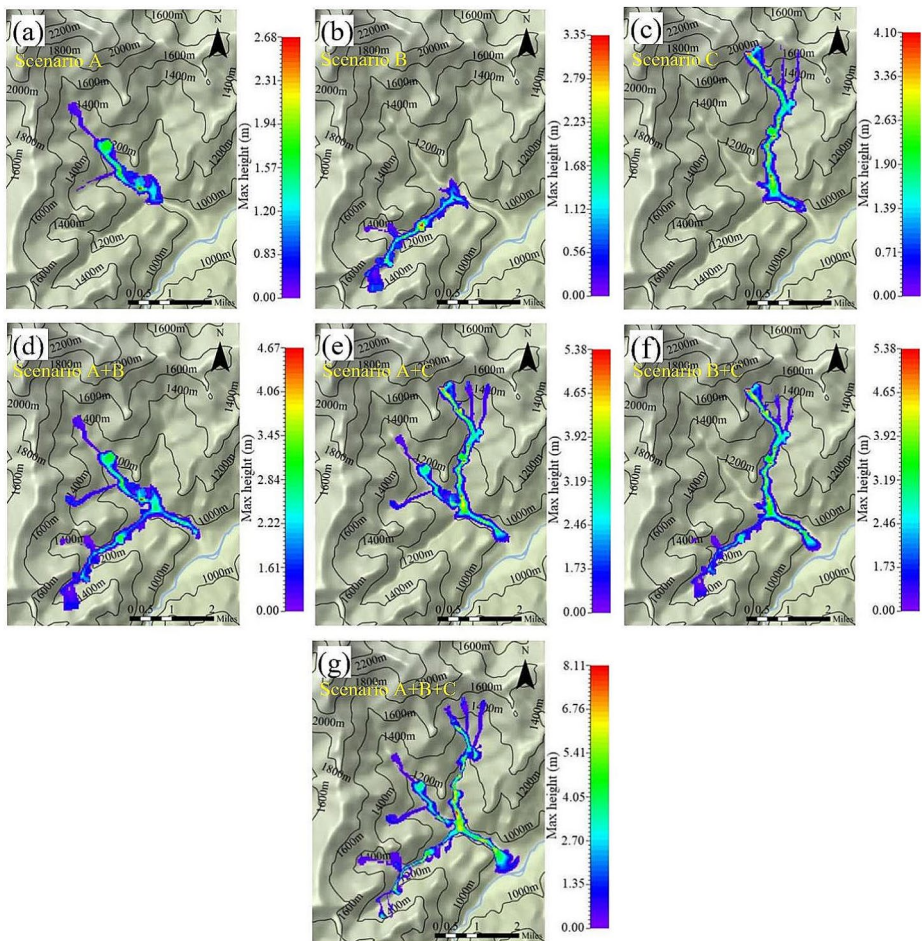


Fig. 7 Niutanggou debris flow simulation results. (a), (b), and (c) depict the debris flow conditions when debris flow occurs individually in the A, B, and C gullies; (d), (e), and (f) represent the debris flow conditions upon the confluence of two gullies; (g) represents the debris flow conditions in the three-gully confluence scenario

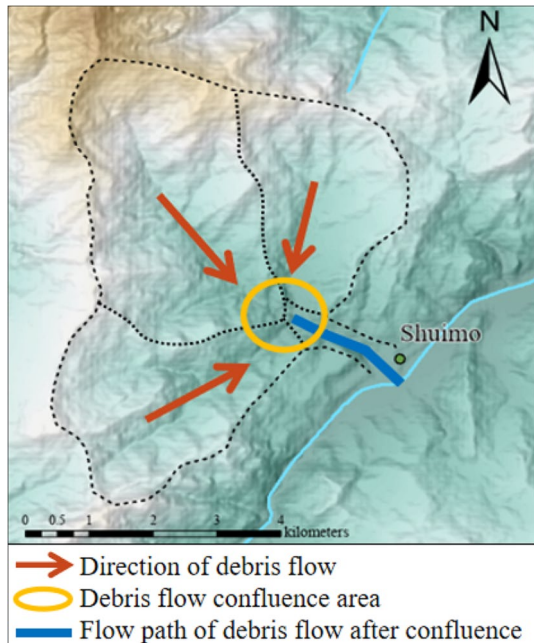
distance and accumulation height of debris flows are greater when multiple gullies experience simultaneous eruptions compared to when debris flows occur individually in each gully. Simultaneous debris flows from multiple gullies exhibit an amplification effect. Specifically, the amplification effect on debris flow height is as follows: debris flows originating from three gullies have a greater height than those from any two gullies or from a single gully, while debris flows from two gullies exceed the height of those from a single gully. This phenomenon may be attributed to the increased total volume of debris flow material (Iverson 1997) and the confluence effects among the gullies.

The downstream gully debris flow velocities under the seven scenarios are shown in Fig. 10. Prior research has suggested that the velocity of debris flows is typically positively correlated with their volume (Melo et al. 2018). However, Fig. 10 illustrates that the velocity in the B+C scenario is lower than that in scenario A+C. This indicates that the variation in velocity upon debris flow confluence is more complex than the simple additive height accumulation of the debris flows.

In order to deeply analyze the movement characteristics of debris flows when multiple gullies occur simultaneously, we further summarize and organize the data in Figs. 9 and 10. The highest level of debris flow accumulation and the highest speed at which the debris flow moves within the confluence area (0–200 m channel range) were estimated for various scenarios and plotted as shown in Fig. 11.

Figure 11 illustrates that after the confluence of flows A and B, the accumulation height of the debris flow at the confluence point increased ($H_{A+B} = 1.7\text{ m} > H_A = 0.9\text{ m} > H_B = 1.3\text{ m}$). Additionally, the velocity was significantly lower compared to that when A or B erupted independently ($V_{A+B} = 1.5\text{ m/s} < V_A = 2.5\text{ m/s} < V_B = 2.8\text{ m/s}$). This occurred because the angle between channels A and B was approximately 90° , leading to a substantial uprush effect upon the confluence of the debris flows from the two channels. This caused the flow

Fig. 8 Scheme for obtaining simulated motion data for debris flow



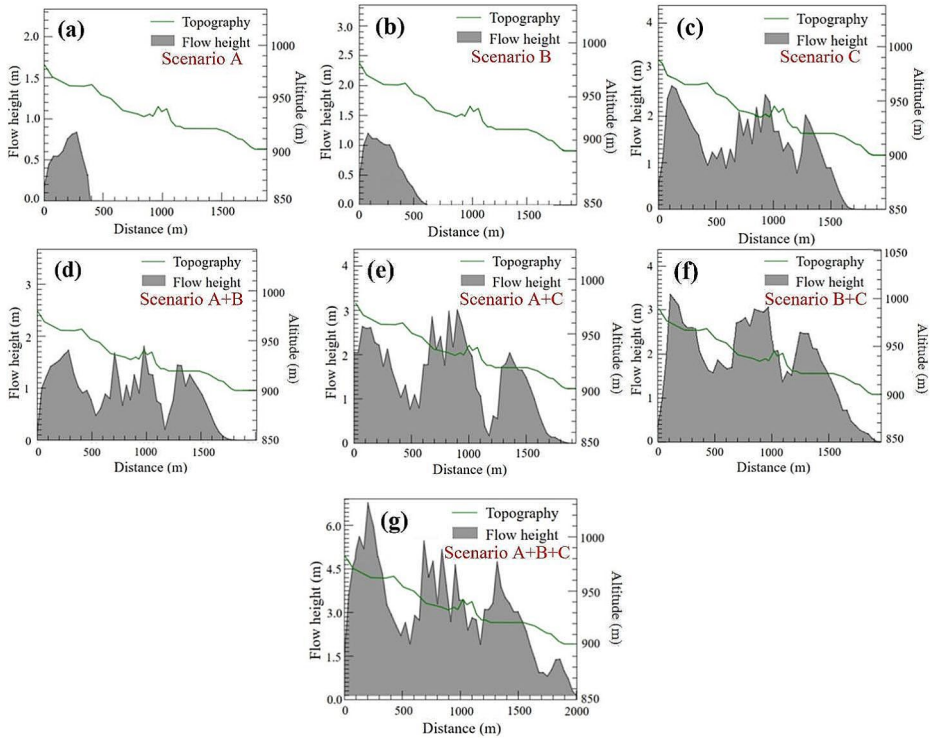


Fig. 9 Influence of confluence on the debris flow height. (a), (b), and (c) depict the debris flow heights when debris flows occur individually in the A, B, and C gullies; (d), (e), and (f) represent the debris flow heights upon two-gully confluence scenarios; (g) represents the debris flow height in the three-gully confluence scenario

height to increase and the velocity to drop. Similarly, owing to the relatively large angle between channels B and C ($\angle BC = 130^\circ$), a substantial uprush effect occurred during confluence. Compared to the effects following the independent eruption of channel C, the convergence of channels C and B led to an increase in debris flow height and a decrease in velocity ($V_{B+C} = 3.2 \text{ m/s} < V_C = 3.8 \text{ m/s}$). This observation aligns with the findings of Zhang et al. (2018), who conducted velocity and discharge analyses on multiple cross-sections of the Longtan Gully in Miyun City. Moreover, Fig. 11 shows that when channels A and C erupted simultaneously and converged, the accumulation height of the debris flow did not markedly increase or differ from that obtained when channel C erupted independently. However, after the confluence of channels B and C, the accumulation height increased substantially. This outcome occurred because the confluence angle between B and C was larger than that between A and C ($\angle BC = 130^\circ > \angle AC = 40^\circ$), resulting in a larger uprush effect during confluence, leading to a decrease in velocity ($V_{B+C} = 3.2 \text{ m/s} < V_C = 3.8 \text{ m/s}$) and more material accumulating at the confluence point. In contrast, when channels A and C converged, the uprush effect was less pronounced, and after confluence, the material flowed downstream with a relatively high velocity, even exceeding that when channel C erupted independently ($V_{A+C} = 4.7 \text{ m/s} > V_C = 3.8 \text{ m/s}$). However, these findings differed from those of Zhang et al. (2018), likely because when the angle between the two branches is small, the uprush

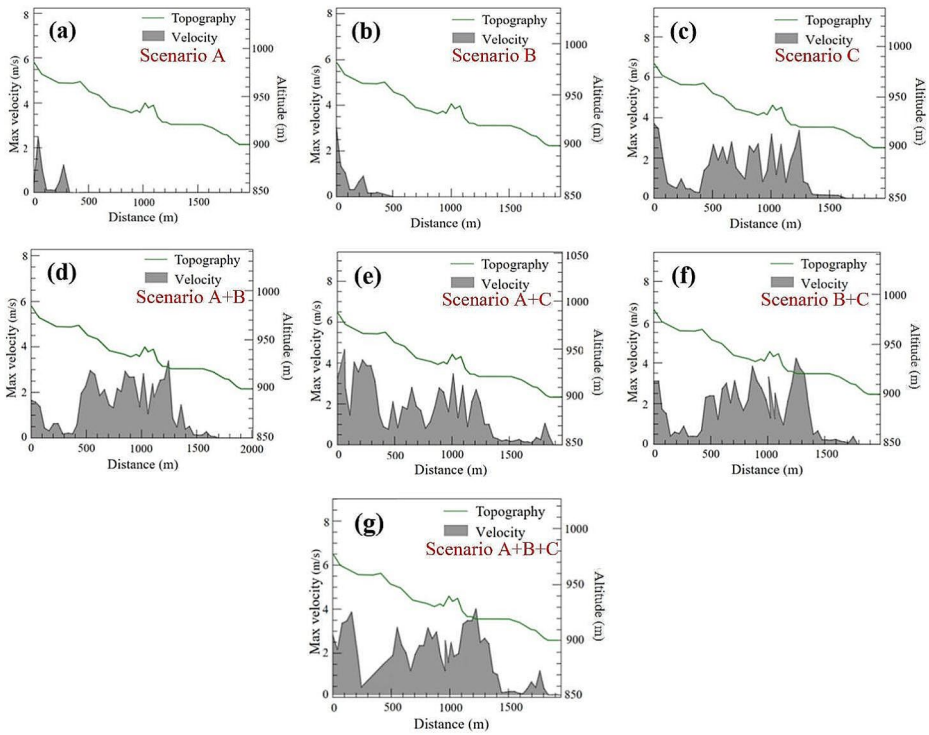


Fig. 10 Influence of confluence on the debris flow velocity. (a), (b), and (c) represent the debris flow velocities when debris flows occur individually in the A, B, and C gullies; (d), (e), and (f) represent the debris flow velocities upon two-gully confluence scenarios; (g) represents the debris flow velocity in the three-gully confluence scenario

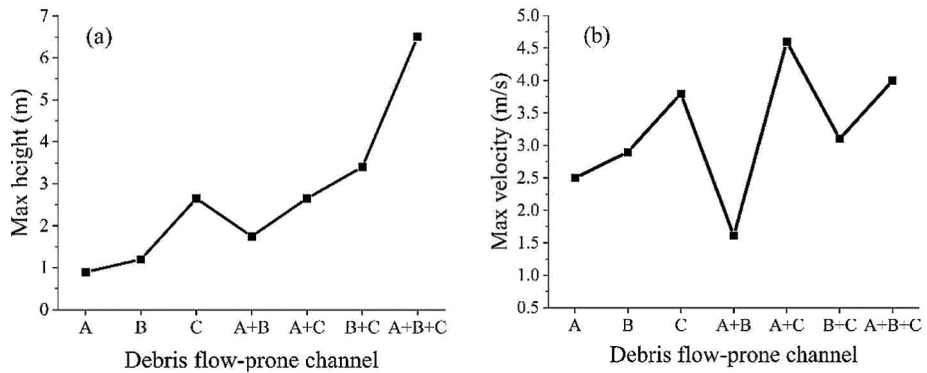


Fig. 11 Statistical analysis of the maximum height (a) and velocity (b) of debris flows in the confluence area. A, ShanWangMiao Gully; B, Liansanpo Gully; and C, Niutang Gully

effect is less pronounced and the debris flow exhibits larger volume and better mobility after confluence (Iverson 1997).

In general, the fluidity of debris flow is directly related to its total volume. A larger debris flow volume corresponds to improved fluidity. Figure 11 reveals phenomena that warrant further investigation. In Fig. 11a, the flow height in the A+C scenario is nearly identical to the height observed when debris flow occurs solely in the C gully, despite the fact that the debris flow source volume in the A+C scenario is 2.6 times greater than that in the C gully scenario. In Fig. 11b, the debris flow velocity in the A+B scenario is notably lower than in both the A and B scenarios. Similarly, the B+C scenario exhibits the same characteristics, with its velocity being lower than that in the C scenario.

4.2 Simulation of the influence of confluence angle on debris flow

Observations of the topographic characteristics of the Niutanggou debris flow suggest that the angle between tributaries may be a key factor influencing the movement characteristics of debris flows following the confluence of multiple tributaries. Subsequently, additional simulation experiments will be conducted with the angle between tributaries as the sole variable to examine its impact on the movement characteristics of debris flows.

RAMMS was employed to simulate the confluence movement of two channels at different confluence angles β , where the confluence angles were set at 10°, 30°, 70°, and 90°. This was to show how the confluence angle impacts the movement characteristics of debris flows after they have been confluenced (Fig. 12). Throughout the simulation, the slopes of both channels were 30°, the debris flow had a density of 2000 kg/m³, the volume and release height of the debris source remained constant, the turbulent coefficient ξ and dry friction coefficient μ were still set to 700 and 0.09, and the erosion function was not activated during this simulation. Upon the automatic completion of the simulation, data on the maximum flow height and maximum flow velocity of the debris flow within the flume were collected throughout the entire movement process.

The simulation results for the flume are shown in Figs. 13 and 14. Figure 13 depicts the maximum accumulation height of debris flow convergence at different intersection angles. In particular, as the intersection angle increases, the maximum width of the accumulation fan decreases, whereas the maximum length increases. The primary reason for this phenomenon is that as the confluence angle increases, a lateral collision occurs when debris flows from the two channels converge, leading to a dissipation of kinetic energy and a consequent reduction in the lateral velocity of the debris flow. A larger confluence angle results in a more pronounced reduction in lateral kinetic energy. Moreover, when the angle at which the flume intersects increases, the height at which the debris flow accumulates in the confluence area also increases gradually (indicated by a color shift from blue to cyan in the confluence area).

Figure 14 illustrates the velocity profile of the debris flow when the sediment was released simultaneously from the two flumes at different intersection angles. The results showed that the debris flow exhibited higher velocities while moving within the flumes, whereas its speed gradually diminished upon exiting the flumes. As the intersection angle increased, the lateral velocity of the debris flow in the confluence area gradually decreased. Although the longitudinal velocity of the debris flow did not increase, the color intensity of the longitudinal velocity field increased. This could be attributed to the enhanced quantity

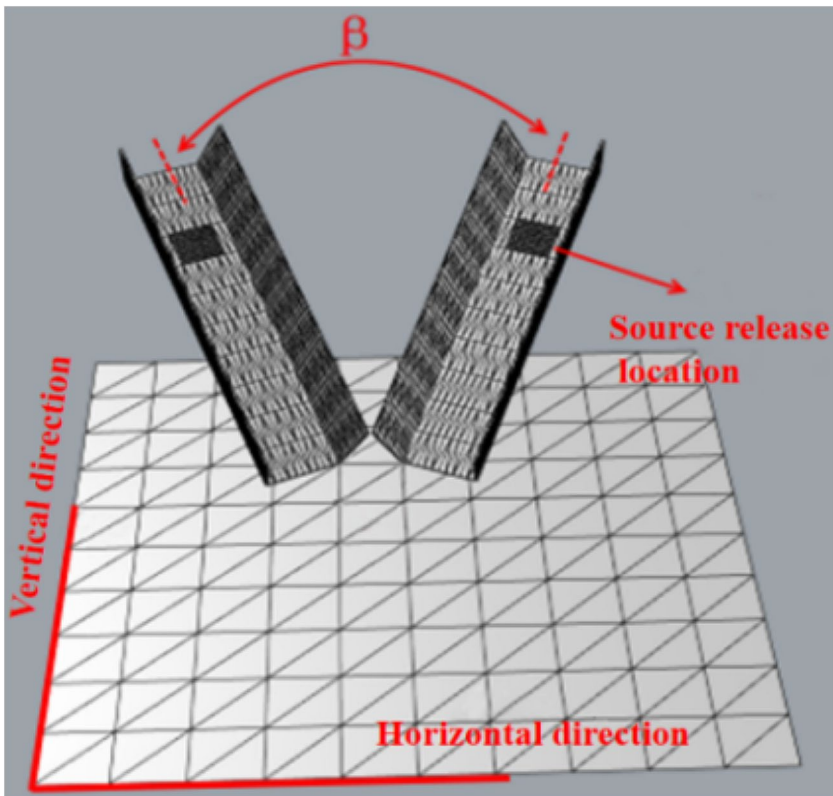


Fig. 12 Debris-flow flume and the depositional plate. The black area indicates the volume and release height of each debris source

of debris flow moving in the longitudinal direction during confluence, indicating that the primary component of the debris-flow velocity that was counteracted during confluence was in the lateral direction. Moreover, an uprush effect was observed during debris-flow confluence: the velocities were smaller at the center of the confluence area, with regions of even zero velocity (depicted by the white area at the confluence focal point). Furthermore, with the increase in the confluence angle, the area of the white region increased.

Figure 15 displays the maximum height and the area of the zero-velocity (white) region during the flume simulation of convergence from various angles. Previous studies have shown that debris flow confluence substantially affects the characteristics of debris flow movement (Chen et al. 2000; Stancanelli et al. 2014, 2015; Zhang et al. 2018). Notably, the results from flume simulations consistently support that when debris flows converge in channels, an amplification effect occurs on the deposition height following confluence. Moreover, this effect is related to the angle between the converging channels (Dang et al. 2009; Stancanelli et al. 2014, 2015; Zhang et al. 2018) as the confluence angle increases, the amplification effect on the deposition height becomes more pronounced, and the velocity of debris flow in the confluence area decreases. Additionally, we found that as the confluence angle increased, there was a gradual decrease in the maximum width of the debris

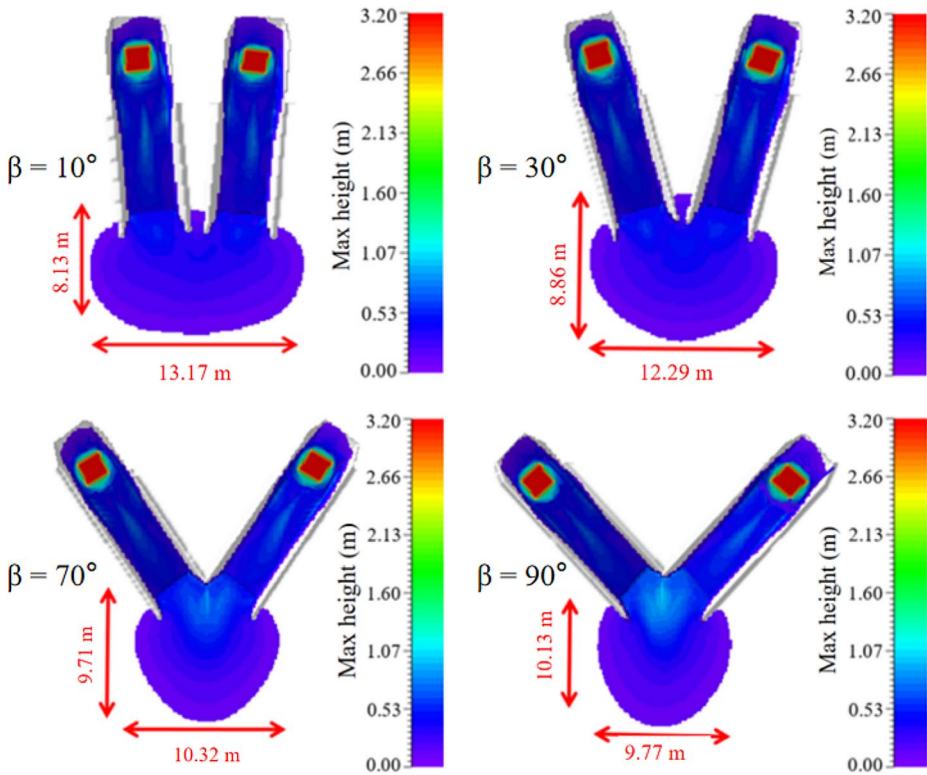


Fig. 13 Flow height of debris flows under different confluence angles

flow deposition fans. At the same time, the runoff distance increased, which aligns with the findings of Ye et al. (2016).

5 Conclusions

Debris flow is a globally common geological event with social impacts. This study utilized a numerical simulation methodology to examine the patterns of variation in the movement characteristics of debris flows under confluence conditions. Subsequently, seven different scenarios were evaluated using this approach based on relevant data from the Niutang Gully debris flow under various confluence conditions. Additionally, simulated flume experiments were conducted to compare and validate the confluence simulation results of the Niutang Gully debris flow, which led to the following conclusions:

1. In the confluence areas of debris flows within channels, the flow distance, depth, and velocity changed during the confluence process. As the number of confluence gullies increased, the flow height increased.
2. The confluence angle had an impact on both the velocity and depth of the debris flows at the confluence point. As the confluence angle increased, it led to a larger hydraulic jump

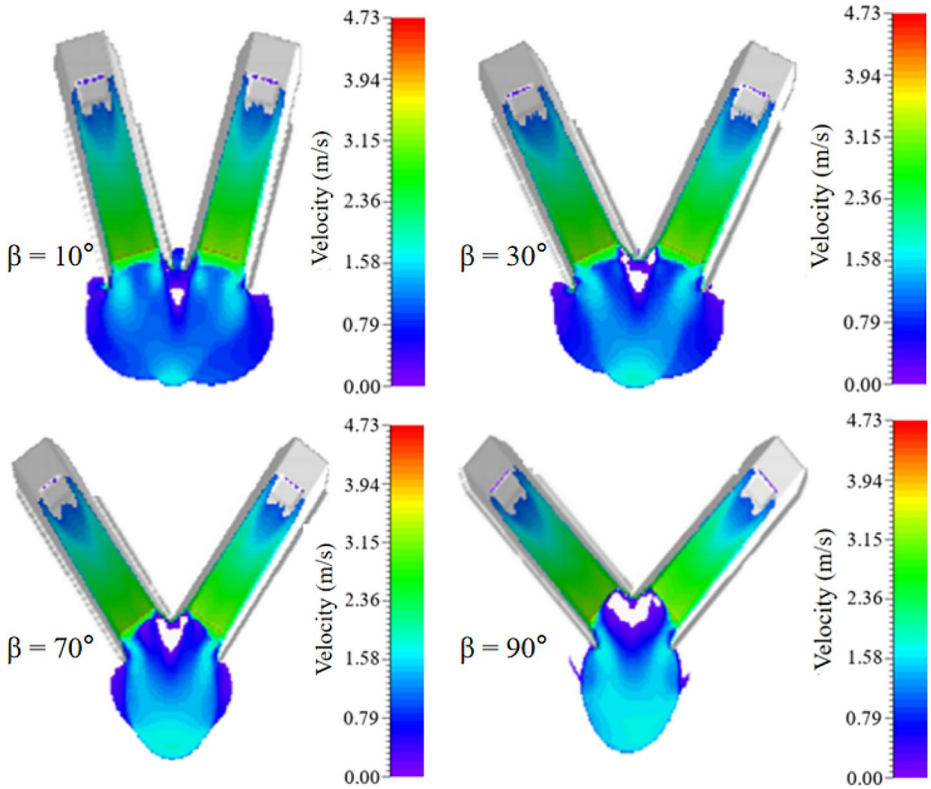
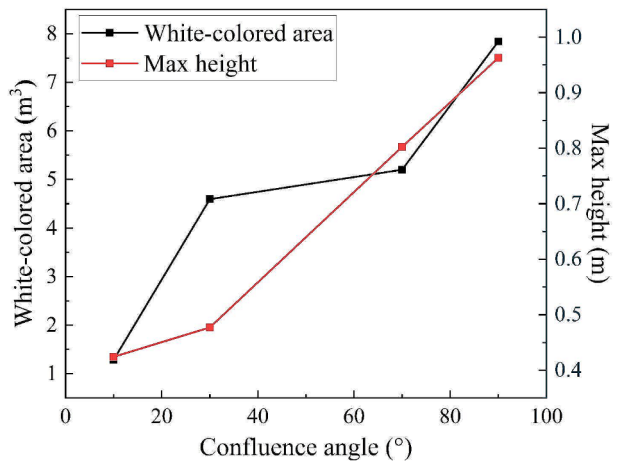


Fig. 14 Velocity of the debris flows converging at different confluence angles

Fig. 15 Statistical analysis of the zero-velocity (white region) area and maximum height in the flume simulation results



effect at the confluence point, resulting in a decrease in the velocity of the debris flow and a more substantial amplification effect on the accumulation height in the confluence area.

However, owing to limitations in the simulation software and research methods, this study did not account for changes in the impact force and erosion capacity of debris flows after confluence. This aspect of the research will be refined in future studies. Together, our findings on variations in motion characteristics during the confluence of debris flows will serve as a reference for the design and planning of debris flow protection projects. In addition, they establish a foundation for further investigation of the movement processes of mass-flow debris flows in complex terrain environments.

Author contributions All authors contributed to the study conception and design. Material preparation, data collection, and analysis were performed by HW, JZ, and QH. WL and LM participated in planning and supervision. The first draft of the manuscript was written by JZ; all authors commented on previous versions of the manuscript. All the authors have read and approved the final manuscript.

Funding This work was supported by the National Key R&D program of China (2023YFC3008300), the Original Innovation Program of the Chinese Academy of Sciences (ZDBS-LY-DQC039), the National Natural Science Foundation of China (42277179), the Science and Technology Research Program of Institute of Mountain Hazards and Environment, the Chinese Academy of Sciences (IMHEZYTS-04, IMHE-CXTD-02), and the Youth Innovation Promotion Association of the Chinese Academy of Sciences (2021373).

Declarations

Conflict of interest The authors have no competing interests to declare that are relevant to the content of this article.

References

- Chang M, Tang C, Van Asch TWJ, Cai F (2017) Hazard assessment of debris flows in the Wenchuan earthquake-stricken area, South West China. *Landslides* 14:1783–1792. <https://doi.org/10.1007/s10346-017-0824-9>
- Chen DM (2000) Mechanism of confluence between debris flow and the main river. Dissertation, Chinese Academy of Water Conservancy Science
- Chen J, He YP, Wei FQ (2005) Debris flow erosion and deposition in Jiangjia Gully, Yunnan, China. *Environ Geol* 48:771–777. <https://doi.org/10.1007/s00254-005-0017-z>
- Chen HX, Zhang LM, Gao L, Yuan Q, Lu T, Xiang B, Zhuang WL (2017) Simulation of interactions among multiple debris flows. *Landslides* 14:595–615. <https://doi.org/10.1007/s10346-016-0710-x>
- Chen Y, Qiu Z, Li B, Yang Z (2018) Numerical simulation on the dynamic characteristics of a tremendous debris flow in Sichuan. *China Processes* 6(8):109. <https://doi.org/10.3390/pr6080109>
- Cheng D, Cui Y, Su F, Jia Y, Choi CE (2018) The characteristics of the Mocoa compound disaster event. *Colombia Landslides* 15:1223–1232. <https://doi.org/10.1007/s10346-018-0969-1>
- Christen M, Kowalski J, Bartelt P (2010) RAMMS: Numerical simulation of dense snow avalanches in three-dimensional terrain. *Cold Reg Sci Technol* 63(1–2):1–14. <https://doi.org/10.1016/j.coldregions.2010.04.005>
- Cui P, Guo X, Yan Y, Li Y, Ge Y (2018) Real-time observation of an active debris flow watershed in the Wenchuan Earthquake area. *Geomorphology* 321:153–166. <https://doi.org/10.1016/j.geomorph.2018.08.024>
- Dang C, Cui P, Cheng ZL (2009) The formation and failure of debris flow-dams, background, key factors and model tests: case studies from China. *Environ Geol* 57:1901–1910. <https://doi.org/10.1007/s00254-008-1479-6>

- Deubelbeiss Y, Graf C (2013) Two different starting conditions in numerical debris flow models—case study at Dorfbach, Randa (Valais, Switzerland). In: Graf C (ed) *Mattertal—Ein Tal in Bewegung*. Eidg. Forschungsanstalt für Wald, Schnee und Landschaft WSL, Birmensdorf, pp 125–138
- Ding XY, Hu WJ, Liu F, Yang X (2023) Risk assessment of debris flow disaster in mountainous area of northern Yunnan Province based on FLO-2D under the influence of extreme rainfall. *Front Environ Sci* 11:1252206. <https://doi.org/10.3389/fenvs.2023.1252206>
- Du C (2021) Deposition pattern of stony and muddy debris flow at the confluence area. *J Mt Sci* 18:622–634. <https://doi.org/10.1007/s11629-020-6046-y>
- Du C, Yao LK, Shakya S, Li LG, Sun XD (2014) Damming of large river by debris flow: dynamic process and particle composition. *J Mt Sci* 11:634–643. <https://doi.org/10.1007/s11629-012-2568-2>
- Guo X, Li Y, Cui P, Yan H, Zhuang J (2020) Intermittent viscous debris flow formation in Jiangjia Gully from the perspectives of hydrological processes and material supply. *J Hydrol* 589:125184. <https://doi.org/10.1016/j.jhydrol.2020.125184>
- Horton AJ, Hales TC, Ouyang C, Fan X (2019) Identifying post-earthquake debris flow hazard using Mass-flow. *Eng Geol* 258:105134. <https://doi.org/10.1016/j.enggeo.2019.05.011>
- Iverson RM (1997) The physics of debris flows. *Rev Geophys* 35(3):245–296. <https://doi.org/10.1029/97RG00426>
- Li Y, Liu J, Su F, Xie J, Wang B (2015) Relationship between grain composition and debris flow characteristics: a case study of the Jiangjia Gully in China. *Landslides* 12:19–28. <https://doi.org/10.1007/s10346-014-0475-z>
- Lin JY, Yang MD, Lin BR, Lin PS (2011) Risk assessment of debris flows in Songhe Stream. *Taiwan Eng Geol* 123(1–2):100–112. <https://doi.org/10.1016/j.enggeo.2011.07.003>
- Liu B, Hu X, Ma G, He K, Wu M, Liu D (2021a) Back calculation and hazard prediction of a debris flow in Wenchuan meizoseismal area, China. *Bull Eng Geol Environ* 80:3457–3474. <https://doi.org/10.1007/s10064-021-02127-3>
- Liu J, Li C, Ma C, Li Q (2021b) Depositional morphology of debris flow in the junction with mainstream channel. *IOP Conf Ser Earth Environ Sci* 861(6):062044. <https://doi.org/10.1088/1755-1315/861/6/062044>
- Ma Z, Liu J (2022) Dynamic simulation and analysis of large-scale debris flow field. *Geofluids*, 2022:2663551. <https://doi.org/10.1155/2022/2663551>
- Ma C, Hu K-H, Zou Q, Tian M (2013) Characteristics of clustering debris flows in Wenchuan earthquake zone. *J Mt Sci* 10:953–961. <https://doi.org/10.1007/s11629-013-2410-5>
- Melo R, van Asch T, Zêzere JL (2018) Debris flow run-out simulation and analysis using a dynamic model. *Nat Hazard Earth Sys Sci* 18(2):555–570. <https://doi.org/10.5194/nhess-18-555-2018>
- Mikoš M, Bezak N (2021) Debris flow modelling using RAMMS model in the alpine environment with focus on the model parameters and main characteristics. *Front Earth Sci* 8:605061. <https://doi.org/10.3389/feart.2020.605061>
- Ouyang C, Wang Z, An H, Liu X, Wang D (2019) An example of a hazard and risk assessment for debris flows—A case study of Niwan Gully, Wudu, China. *Eng Geol* 263:105351. <https://doi.org/10.1016/j.enggeo.2019.105351>
- Silva GD, Roberts DA, McFadden JP, King JY (2022) Shifts in salt marsh vegetation landcover after debris flow deposition. *Remote Sens* 14(12):2819. <https://doi.org/10.3390/rs14122819>
- Stancanelli LM, Lanzoni S, Foti E (2014) Mutual interference of two debris flow deposits delivered in a downstream river reach. *J Mt Sci* 11:1385–1395. <https://doi.org/10.1007/s11629-014-3051-z>
- Stancanelli LM, Lanzoni S, Foti E (2015) Propagation and deposition of stony debris flows at channel confluences. *Water Resour Res* 51(7):5100–5116. <https://doi.org/10.1002/2015WR017116>
- Tang C, Rengers NV, van Asch TWJ, Yang YH, Wang GF (2011) Triggering conditions and depositional characteristics of a disastrous debris flow event in Zhouqu City, Gansu Province, northwestern China. *Nat Hazard Earth Sys Sci* 11(11):2903–2912. <https://doi.org/10.5194/nhess-11-2903-2011>
- Trujillo-Vela MG, Ramos-Cañón AM, Escobar-Vargas JA, Galindo-Torres SA (2022) An overview of debris-flow mathematical modelling. *Earth-Sci Rev* 232:104135. <https://doi.org/10.1016/j.earscirev.2022.104135>
- Wang GL (2013) Lessons learned from protective measures associated with the 2010 Zhouqu debris flow disaster in China. *Nat Hazards* 69:1835–1847. <https://doi.org/10.1007/s11069-013-0772-1>
- Wang J, Yang S, Ou G, Gong Q, Yuan S (2018) Debris flow hazard assessment by combining numerical simulation and land utilization. *Bull Eng Geol Environ* 77:13–27. <https://doi.org/10.1007/s10064-017-1006-7>
- Wang C, Hu X, Hu K, Liu S, Zhong W (2022a) Impact assessment of the Ms7. 0 earthquake on Jiuzhaigou Valley from the perspective of vegetation net primary productivity. *Sens (Basel)* 22(22):8875. <https://doi.org/10.3390/s22228875>
- Wang H, Dai L, Pan D, Yue J, Fu D, Yan T (2022b) Dynamic numerical simulation and risk predictive assessment of the slope debris flow for the rear mountain at the management office of the Erlang Mountain Tunnel. *Front Earth Sci* 10:1025636. <https://doi.org/10.3389/feart.2022.1025636>

- Wang J, Hassan MA, Saletti M, Yang X, Zhou H, Zhou J (2022c) Experimental study on the mitigation effects of deflection walls on debris flow hazards at the confluence of tributary and main river. *Bull Eng Geol Environ* 81(9):354. <https://doi.org/10.1007/s10064-022-02850-5>
- Yang Z, Zhao X, Chen M, Zhang J, Yang Y, Chen W, Bai X, Wang M, Wu Q (2023) Characteristics, dynamic analyses and hazard assessment of debris flows in Niuniangou Valley of Wenchuan County. *Appl Sci* 13(2):1161. <https://doi.org/10.3390/app13021161>
- Ye J, Chen J, Chen X, Xhu J, Xu Z (2016) Numerical simulation study on hazardous area for the confluence deposit of gully debris flow. *Sci Geogr Sin* 36(10):1588–1594
- Zhang N, Matsushima T (2016) Simulation of rainfall-induced debris flow considering material entrainment. *Eng Geol* 214:107–115. <https://doi.org/10.1016/j.enggeo.2016.10.005>
- Zhang Y, Wang P, Wu B, Hou S (2015) An experimental study of fluvial processes at asymmetrical river confluences with hyperconcentrated tributary flows. *Geomorphology* 230:26–36. <https://doi.org/10.1016/j.geomorph.2014.11.001>
- Zhang YX, Ma C, Yang HL, Ni SB (2018) Causes and dynamic characteristics of debris flow disaster in Longtangou Watershed, Miyun County of Beijing. *J Beijing Univ* 40(7):73–84

Publisher's Note Springer Nature remains neutral with regard to jurisdictional claims in published maps and institutional affiliations.

Springer Nature or its licensor (e.g. a society or other partner) holds exclusive rights to this article under a publishing agreement with the author(s) or other rightsholder(s); author self-archiving of the accepted manuscript version of this article is solely governed by the terms of such publishing agreement and applicable law.